# Identification of a primordial high D/H component in the matrix of unequilibrated ordinary chondrites

Helen Grant, Romain Tartèse, Rhian Jones, Laurette Piani, Yves Marrocchi

Geochimica et Cosmochimica Acta 378 (2024) 58–70

Contents lists available at ScienceDirect

Geochimica et Cosmochimica Acta

journal homepage: www.elsevier.com/locate/gca

# Identification of a primordial high D/H component in the matrix of unequilibrated ordinary chondrites

Helen Grant [a,b,*], Romain Tartèse [a], Rhian Jones [a], Laurette Piani [c], Yves Marrocchi [c]

[a] Department of Earth and Environmental Sciences, The University of Manchester, Manchester M13 9PL, UK
[b] Istituto di Astrofisica e Planetologia Spaziali - INAF, Roma, Italy
[c] CRPG, CNRS-Université de Lorraine, UMR 7358, Vandoeuvre les Nancy, France

ARTICLE INFO

*Associate editor:* Martin Robert Lee

*Keywords:*
Unequilibrated ordinary chondrites
D/H ratios
Matrix
Secondary ion mass spectrometry
Water
Amorphous silicates

ABSTRACT

Deuterium to hydrogen isotope ratios in unequilibrated ordinary chondrites (UOCs) which have undergone little-to-no thermal metamorphism pose an interesting problem when looking at water in the early Solar System. Bulk chondrite studies have shown that UOCs of the lowest subtypes have D/H ratios as high as comets from the outer Solar System, which, along with bulk UOC water abundances, decrease with thermal metamorphism. Since bulk UOC analyses represent a complex mixture of organic and hydrated phases, it is not clear what phase(s) is responsible for the high bulk D/H values. In this study, we report *in situ* secondary ion mass spectrometry (SIMS) measurements of the H isotope composition of the fine-grained matrix of UOCs with petrological subtypes ranging from 3.00 to 3.9. We find that for matrix areas in UOCs of petrologic subtype ≥3.2, correlations between D-rich organic material and D-poor phyllosilicates give relatively D-poor intrinsic water isotopic compositions, with δD values between −320 ± 91 ‰ and −71 ± 71 ‰, which are inherited from parent body accretion. Therefore, we conclude that OC parent bodies accreted D-poor water ice that had an H isotopic composition similar to that of CM and CV chondrite parent bodies. We find that matrix in UOCs of the lowest subtypes (Semarkona, Bishunpur, and Ngawi) show similar water and organic H isotope compositions to higher type UOCs. Our *in situ* analyses also show that matrix areas in these pristine UOCs contain a third, thus far unidentified, component that carries the high D/H signature, with δD values up to ~6000 ‰. We propose that this component is pristine amorphous silicates preserved from the molecular cloud or early protoplanetary disc that is extremely sensitive to thermal and aqueous alteration on asteroidal parent bodies.

## 1. Introduction

Unequilibrated ordinary chondrites (UOCs) are primitive ordinary chondrites that have undergone minimal modification since their asteroidal parent bodies formed around 4.5 billion years ago, early in the history of the Solar System. These meteorites are composed of high-temperature components such as chondrules and minor amounts of calcium- and aluminium-rich inclusions (CAIs), which are set in a porous, fine-grained (<μm) matrix. Matrix in UOCs is a complex mixture of anhydrous silicates, and small amounts of organics and hydrated compounds (e.g., Alexander et al., 1989; Scott and Krot, 2014; Dobrică and Brearley, 2020a, 2020b). In the most primitive UOCs, the matrix contains amorphous silicates as well as phases indicative of aqueous alteration on the UOC asteroid parent bodies, such as phyllosilicates, amphiboles, fayalite, and magnetite (e.g., Alexander et al., 1989, 2012; Dobrică and Brearley, 2014, 2020; Krot et al., 2022, Zanetta et al., 2022). Despite matrix only comprising ~10–15 wt% of bulk UOCs (Weisberg et al., 2006), studies of UOCs have measured bulk water abundances of up to ca. 1 wt% $H_2O$ in samples of the lowest petrologic subtype (Alexander et al., 2010; Vacher et al., 2020; Marrocchi et al., 2020; Grant et al., 2023). These observations indicate that water was present in OC parent asteroids, presumably as a result of melting of accreted ice.

In addition to the clear evidence for the presence of hydrated material in the least metamorphosed UOCs, these samples are characterised by elevated bulk hydrogen isotope ratios. UOCs with subtype < 3.2 have bulk D/H ratios of up to *ca.* $700 \times 10^{-6}$ (Robert et al., 1979, 1987; McNaughton et al., 1981, 1982; Yang and Epstein, 1983; Robert et al., 1987; Alexander et al., 2012; Grant et al., 2023), significantly higher than the standard mean value of ocean water on Earth, $155.76 \times 10^{-6}$.

* Corresponding author.
*E-mail addresses:* helen.grant@manchester.ac.uk, helen.grant@inaf.it (H. Grant).

https://doi.org/10.1016/j.gca.2024.06.005
Received 2 February 2024; Accepted 5 June 2024
Available online 14 June 2024

The bulk UOC D/H ratios are also considerably higher than the bulk D/H ratios measured in volatile-rich carbonaceous (CM, CR, CI) chondrites (~150–250 × $10^{-6}$; Alexander et al., 2012; Vacher et al., 2020; Marrocchi et al., 2021). Hydrogen isotopes are often used as a tracer for the origin and transport of water/ice in the early Solar System, notably because of the large isotopic variations observed between different objects. There were at least two carriers of water in the early Solar System: pristine D-rich ice grains originating from the molecular cloud and/or outer Solar System and D-poor water formed via rapid isotopic exchange between D-rich water vapour and D-depleted $H_2$ molecules in the warm inner Solar System (Jacquet and Robert, 2013; Yang et al., 2013). To a first order, mixing between these D-poor and D-rich carriers would have resulted in water D/H approximately increasing with heliocentric distance from the Sun (e.g., Drouart et al., 1999; Alexander et al., 2012; Jacquet and Robert, 2013; Yang et al., 2013; Piani et al., 2021; Müller et al., 2022). However, since UOC parent asteroids are thought to have formed closer to the Sun than those of carbonaceous chondrites (Scott et al., 2018), the observation that pristine UOCs have higher bulk D/H ratios than water-rich chondrites such as those from the CM, CR, and CI groups is difficult to explain.

However, there is an important complexity to the D/H carrier in UOCs. Similar to carbonaceous chondrites, the fine-grained matrix in which most of the water is hosted contains other H-bearing components, such as carbonaceous organic matter (e.g., Alexander et al., 2007, 2012; Piani et al., 2021). Therefore, bulk D/H ratios represent mixed H isotope signatures of at least two H-bearing components and are not directly representative of the D/H ratios of the water ice accreted by the UOC parent bodies. Due to the small grain sizes and heterogeneous mixing at the nanoscale, it is not straightforward to physically separate water-bearing silicates from organics to measure their bulk D/H ratios independently. In order to disentangle water and organic H isotope compositions, and to further characterise the D/H ratio of water accreted to the UOC parent bodies, it is necessary to examine the sample with high-resolution *in situ* techniques. *In situ* analyses of matrix areas in Semarkona suggested that the D-rich component is not related to organic material, but instead to phyllosilicates (Piani et al., 2015). To expand this limited dataset, we carried out *in situ* petrological and isotopic analyses of fine-grained matrix areas of 13 UOCs using scanning electron microscopy (SEM), electron probe microanalyses (EPMA), and secondary ion mass spectrometry (SIMS). All samples are falls that have undergone minimal, if any, terrestrial alteration, and for which we previously determined the bulk H isotope compositions (Grant et al., 2023).

## 2. Materials and methods

### 2.1. Samples

We conducted *in situ* analyses on the following 13 UOC fall samples: Aba Panu (eBay), Bishunpur (BM.80339), Bremervörde (BM.33910), Ceniceros (BM.1989,M31), Chainpur (BM.1915,86), Krymka (BM.1956,325), Mezö-Madaras (BM.33909), Ngawi (USNM 2483), Parnallee (BM.1985,M138), Semarkona (AMNH 4128), Sharps (USNM 640), St Mary's County (USNM 5930), and Tieschitz (BM.2003,M12), all of which were part of the bulk $H_2O$ and H isotope analysis study by Grant et al. (2023). The powders used for bulk analyses in Grant et al. (2023) were prepared from aliquots of the same chips from which polished blocks were prepared for *in situ* analyses. The samples have

**Table 1**
Average chemical compositions of matrix areas of the studied UOCs, determined by EPMA.

| Sample | Ngawi | Semarkona | Bishunpur | Krymka | St Mary's County | Chainpur | Sharps | Parnallee | Aba Panu | Tieschitz | Ceniceros | Mezö-Madaras | Bremervörde |
|---|---|---|---|---|---|---|---|---|---|---|---|---|---|
| Type | LL3.1–3.7 | LL3.00 | LL3.15 | LL3.2 | LL3.3 | LL3.4 | H3.4 | LL3.6 | L3.6 | H/L3.6 | L3.7 | L3.7 | H/L3.9 |
| Source[a] | USNM | AMNH | NHM | NHM | USNM | NHM | USNM | NHM | eBay | NHM | NHM | NHM | NHM |
| N[b] | 15 | 18 | 26 | 24 | 30 | 9 | 17 | 17 | 11 | 24 | 28 | 17 | 27 |
| $SiO_2$ | 34.10 | 35.61 | 42.65 | 31.96 | 34.23 | 22.30 | 32.64 | 38.49 | 43.14 | 32.90 | 35.97 | 43.21 | 39.29 |
| σ[c] | *3.83* | *2.41* | *3.78* | *4.29* | *3.18* | *4.67* | *7.54* | *4.67* | *4.89* | *4.63* | *5.66* | *5.14* | *7.79* |
| $TiO_2$ | 0.07 | 0.07 | 0.08 | 0.07 | 0.09 | 0.06 | 0.06 | 0.11 | 0.11 | 0.12 | 0.09 | 0.08 | 0.11 |
| σ | *0.03* | *0.03* | *0.03* | *0.04* | *0.04* | *0.02* | *0.04* | *0.07* | *0.06* | *0.04* | *0.05* | *0.06* | *0.07* |
| $Al_2O_3$ | 2.45 | 4.52 | 4.72 | 3.29 | 4.36 | 1.69 | 0.90 | 2.50 | 2.99 | 2.35 | 2.21 | 3.15 | 3.56 |
| σ | *1.84* | *0.76* | *1.81* | *1.04* | *1.43* | *1.36* | *0.98* | *1.91* | *2.26* | *1.60* | *1.56* | *1.53* | *2.76* |
| $Cr_2O_3$ | 0.33 | 0.27 | 0.33 | 0.23 | 0.28 | 0.26 | 0.29 | 0.28 | 0.53 | 0.41 | 0.39 | 0.19 | 0.42 |
| σ | *0.10* | *0.07* | *0.11* | *0.07* | *0.13* | *0.29* | *0.25* | *0.16* | *0.80* | *0.19* | *0.13* | *0.26* | *0.25* |
| FeO[d] | 26.85 | 21.82 | 19.73 | 36.43 | 31.11 | 38.84 | 29.48 | 20.92 | 17.12 | 25.97 | 22.95 | 18.37 | 18.49 |
| σ | *8.53* | *3.96* | *6.02* | *7.36* | *7.01* | *9.71* | *10.87* | *3.17* | *2.86* | *4.51* | *6.52* | *2.79* | *8.32* |
| MnO | 0.32 | 0.23 | 0.28 | 0.37 | 0.40 | 0.31 | 0.50 | 0.37 | 0.40 | 0.41 | 0.33 | 0.36 | 0.31 |
| σ | *0.14* | *0.04* | *0.09* | *0.08* | *0.11* | *0.08* | *0.23* | *0.06* | *0.05* | *0.05* | *0.06* | *0.05* | *0.08* |
| MgO | 20.37 | 11.85 | 13.37 | 11.09 | 13.61 | 12.35 | 19.57 | 26.50 | 28.58 | 19.32 | 24.17 | 27.90 | 23.92 |
| σ | *6.35* | *3.55* | *4.55* | *2.98* | *3.02* | *5.59* | *8.55* | *4.11* | *4.87* | *3.82* | *3.29* | *2.57* | *6.02* |
| CaO | 1.91 | 1.41 | 1.20 | 1.59 | 1.24 | 1.37 | 0.73 | 1.66 | 1.81 | 1.44 | 1.58 | 1.72 | 1.53 |
| σ | *1.76* | *1.34* | *1.50* | *2.35* | *2.23* | *2.00* | *1.33* | *4.25* | *3.31* | *2.11* | *4.75* | *2.53* | *2.70* |
| $Na_2O$ | 1.22 | 2.42 | 1.94 | 1.11 | 1.72 | 0.75 | 0.36 | 1.27 | 1.51 | 1.13 | 1.08 | 1.57 | 1.66 |
| σ | *1.01* | *0.56* | *0.65* | *0.39* | *0.80* | *0.53* | *0.33* | *0.94* | *1.22* | *0.90* | *0.87* | *0.78* | *1.31* |
| $K_2O$ | 0.24 | 0.55 | 0.42 | 0.19 | 0.46 | 0.14 | 0.14 | 0.13 | 0.14 | 0.13 | 0.07 | 0.03 | 0.12 |
| σ | *0.23* | *0.19* | *0.16* | *0.09* | *0.21* | *0.08* | *0.15* | *0.10* | *0.13* | *0.09* | *0.05* | *0.01* | *0.13* |
| $P_2O_5$ | 0.24 | 0.13 | 0.17 | 0.22 | 0.20 | 0.25 | 0.25 | 0.67 | 0.22 | 0.23 | 0.22 | 0.34 | 0.26 |
| σ | *0.10* | *0.10* | *0.26* | *0.18* | *0.17* | *0.24* | *0.21* | *2.00* | *0.22* | *0.25* | *0.11* | *0.42* | *0.27* |
| FeNi[d] | 2.03 | 2.39 | 2.94 | 3.69 | 0.81 | 1.95 | 3.35 | 1.62 | 0.13 | 1.25 | 4.16 | 0.78 | 4.35 |
| σ | *1.69* | *1.11* | *1.39* | *1.76* | *0.67* | *1.43* | *2.78* | *1.32* | *0.12* | *1.35* | *1.82* | *1.10* | *2.29* |
| FeS[d] | 2.67 | 3.63 | 3.54 | 0.99 | 1.58 | 2.87 | 1.52 | 0.51 | 0.77 | 2.61 | 0.39 | 0.34 | 1.27 |
| σ | *2.73* | *1.66* | *2.49* | *2.22* | *2.82* | *4.02* | *1.66* | *0.66* | *0.91* | *4.16* | *0.48* | *0.37* | *1.02* |
| Total | 92.80 | 84.91 | 91.37 | 91.22 | 90.09 | 83.15 | 89.80 | 95.04 | 97.44 | 88.28 | 93.61 | 98.03 | 95.29 |

[a] Museum Sources are as follows: USNM = Smithsonian National Museum of Natural History, Washington (USA); AMNH = American of Natural History, New York (USA); NHM = Natural History Museum, London (UK). Source numbers are available in text.
[b] Number of EPMA analyses.
[c] 1σ standard deviation of the mean.
[d] FeNi and FeS are calculated, assuming all Ni is in Fe-Ni metal and all S is in FeS. FeO is calculated from the remaining Fe.

petrologic types ranging from 3.00 to 3.9 and they include H, L, and LL groups (details in Table 1). Of note, Ngawi is classified as LL3.1–3.7 as it is a brecciated chondrite with both LL3.1 and 3.7 subtype lithologies (Sears et al., 1991; Grossman & Brearley, 2005). Due to its high bulk D/H ratio and relatively high bulk water content (δD = 1144 ‰ and $H_2O$ = 0.61 wt%, respectively; Grant et al., 2023), we believe that we are sampling the low subtype lithology and, therefore, we treat our Ngawi sample as an LL3.1. Nevertheless, due to the official petrologic type of the sample being LL3.1–3.7 it appears separate from the rest of the samples in plots and tables. For each meteorite, chips of a few mm across with surface areas between ~ 5 – 15 $mm^2$ were stuck to a glass slide, and first polished using SiC polishing discs with decreasing grit size and isopropyl alcohol as the lubricant, and then polished using 6, 3, 1, and 0.25 μm diamond pastes. After polishing, the chips were demounted from the glass slides using acetone, cleaned for 10 min in isopropyl alcohol in an ultrasonic bath, and pressed into 10 mm diameter indium mounts.

### 2.2. Scanning electron microscopy and electron probe microanalysis

The samples were coated with carbon for electron beam analyses. Textures and mineralogy were examined using an FEI Quanta 650 Scanning Electron Microscope (SEM) equipped with an energy dispersive X-ray spectrometer (EDS) at the University of Manchester, allowing us to produce back-scattered electron (BSE) and elemental X-ray maps for all samples. Multiple flat regions of fine-grained matrix were identified in each of the samples for further investigations. We then measured bulk matrix chemical compositions using Cameca SX 100 and JEOL 8200 electron probe microanalyser (EPMA) instruments at the University of Manchester and the University of New Mexico, respectively. For both instruments, analyses were performed with an accelerating voltage of 15 kV, a beam current of 20nA, and a 10 μm diameter defocused beam. Due to the fine-grained and heterogeneous nature of the matrix, multiple analyses were taken in each area and averaged to produce a mean of the bulk matrix composition. The elements measured, standards used, and peak and background counting times are given in Supp. Table S1. Oxide compositions were corrected using the same method as reported in Huss et al. (1981) and Matsunami (1984), where all elemental Ni and S were assigned to Fe-Ni metal (Fe:Ni compositions of metal for each meteorite group were taken from Gattacceca et al., 2014) and troilite (FeS), respectively, and the required amount of Fe added to those phases. The final FeO abundances were recalculated with contributions to FeS and FeNi subtracted, and totals redetermined. For bulk matrix compositions, reported analyses have total uncertainties of ~ 0.4 – 0.5 wt%, based on the combined uncertainty from each individual oxide contribution. All EPMA data are available in Supp. Table S2.

### 2.3. Secondary ion mass spectrometry

We carried out secondary ion mass spectrometry (SIMS) analyses on regions of fine-grained matrix identified and characterised by SEM and EPMA, on the 13 indium-mounted UOC chips. Regions that contained chondrule or mineral fragments, cracks, holes, or imperfect polishing were avoided. Prior to SIMS analyses, we removed the carbon coat and left the samples overnight in an 80 °C furnace to remove any adsorbed water. The mounts were then gold coated and introduced into the SIMS instrument vacuum system several days before analysis. The vacuum in the analysis chamber during analysis was always $< 5 \times 10^{-9}$ mbar. SIMS analyses were carried out using the CAMECA IMS 1280HR2 instrument in monocollection mode at CRPG-CNRS in Nancy (France) over the course of two weeks in October 2022, following the procedure described in Piani et al. (2018). For analysis, a $Cs^+$ beam accelerated at 10 kV with a variable current between 400 pA to 2 nA for UOC samples and down to 50 pA for the H-rich standards was used to ensure a constant $H^-$ count rate of ~ $1.5 \times 10^5$ c/s. The beam was rastered over 15 × 15 $\mu m^2$ areas and intensities of $^1H^-$, $^2D^-$, $^{13}C^-$, and $^{29}Si^-$ were measured. Before analysis, target areas underwent pre-sputtering at 2.5 nA for 3 min over a region of 30 × 30 $\mu m^2$ to implant $Cs^+$ and remove adsorbed H or surface impurities. Each analysis consisted of 30 cycles of data collection, totalling 30 min per analysis.

The standards used to calibrate the SIMS and subsequently to correct data for instrumental mass fractionation (IMF) are given in Supp. Table S3 and comprised a combination of terrestrial samples, including hydrated minerals (Bamble amphibole, Kipawa amphibole, Ser-12A serpentine), H-bearing glass (Etna-4, M98-47963, M98-35, M98-40, M98-43, Tan25-0, Tan25-2), and a type III kerogen (KerIII). Additionally, D-rich insoluble organic matter (IOM) from GRO 95502 (L3.2, find) and Orgueil (CI1, fall) were also analysed. However, these kerogen and IOM samples were excluded from the calibration due to the varying, unknown, levels of H contamination in these porous materials. Plotting the measured vs. known D/H ratios for the mineral and glass standards resulted in a calibration line corresponding to $(D/H)_{true} = [1.38\ (\pm 0.04) \times (D/H)_{measured}]$ (Supp. Fig. S1). We used this calibration to correct the D/H ratios measured in UOC matrix areas, which are reported here using the δD notation, where $\delta D = [(D/H)_{measured} / (D/H)_{SMOW} - 1] \times 1000$, corresponding to the deviation of D/H ratios from the standard mean ocean water ($D/H_{SMOW} = 155.76 \times 10^{-6}$) in parts per thousand (‰). Due to their porous nature, it is likely that UOC matrix area analyses include some H contamination that cannot be accurately quantified (e.g., Remusat et al., 2016); therefore, the corrected D/H ratios represent minimum D/H ratios. All corrected δD values are reported in Supp. Table S4, together with their 2σ uncertainties, which comprise statistical uncertainties associated with each individual analysis and uncertainty on the D/H IMF calibration propagated in quadrature. Mean δD values for each meteorite are reported in Table 2 with their 1σ standard deviations, which reflect heterogeneity in D/H ratios within samples. For subtypes ≥ 3.2, the $(\delta D)_i$ of the $^{13}C$-free y-axis intercepts were calculated using the modified error weighted least squares algorithm of York et al. (2004) in the IsoplotR toolbox (Vermeesch, 2018); uncertainties are given at the 95 % confidence level, and outliers (between 0 and 2 analyses for each sample, see Table 2) were visually excluded from the regressions (see Supp. Fig. S3).

## 3. Results

### 3.1. Matrix composition

All the studied UOCs contain large (>500 μm diameter) chondrules that dominate the make-up of the samples (e.g. Fig. 1f). Between these chondrules, regions of smaller components such as chondrule fragments and anhydrous grains are observed. There are many smooth larger grains of olivine and pyroxene with sizes ranging between *ca.* 1 and >10 μm. All samples also contain feldspathic phases (albite and anorthite) ~ 5 to 20 μm in size, small Fe,Ni grains (<20 μm), and larger (5–30 μm) sulfides. Fine-grained (sub-micrometer) matrix material occurs between these grains, and includes a mixture of many different components that cannot be easily identified by SEM-EDS.

Examples of matrix areas identified for this study are shown in Fig. 1. In samples of subtypes < 3.5, fine-grained matrix areas were more abundant and easier to observe than in samples that have undergone higher levels of thermal metamorphism. Matrix areas show varying degrees of heterogeneity, even within individual samples. They vary in size from 10s to 100s of μm across, as well as compositionally from fine-grained and homogeneous, to more heterogeneous and 'fluffy' (Fig. 1a-c). In samples with subtypes > 3.5, we relied more heavily on X-ray maps, where regions between larger phases that appeared to contain a heterogeneous mixture of components including olivine, pyroxene, and feldspars, and appeared texturally fine-grained, were assumed to be matrix (Fig. 1d-e).

In Si-Fe-Mg ternary diagrams, there is significant scatter of matrix compositions for most samples (Fig. 2). Our EPMA analyses of

**Table 2**
Matrix average δD, $^{13}C/^{1}H$, and $^{1}H/^{29}Si$ ratios as determined by SIMS, with $(\delta D)_i$ values for intrinsic water determined from D/H vs. $^{13}C/^{1}H$ correlations.

| Meteorite | Type | N[a] | Average ‰ | δD[b] ± | Average $^{13}C/^{1}H$ ($\times10^{-2}$)[c] ± | Average $^{1}H/^{29}Si$[c] ± | $(\delta D)_i$[d] ‰ | ± | Pearson coefficient[e] | Rejected[f] |
|---|---|---|---|---|---|---|---|---|---|---|
| Ngawi | LL3.1–3.7 | 21 | 1785 | 2119 | 1.33 0.88 | 5.29 2.37 | | | | |
| Semarkona | LL3.00 | 27 | 2230 | 1140 | 1.25 0.44 | 13.18 5.56 | | | | |
| Bishunpur | LL3.15 | 34 | 660 | 640 | 0.77 0.42 | 9.89 4.83 | | | | |
| Krymka | LL3.2 | 29 | 50 | 165 | 0.52 0.26 | 15.91 5.29 | −193 | 65 | 0.85 | 1 |
| St Marys County | LL3.3 | 9 | 226 | 462 | 1.80 1.05 | 3.93 1.15 | −320 | 91 | 0.99 | 1 |
| Chainpur | LL3.4 | 14 | −58 | 147 | 0.56 0.50 | 19.56 19.48 | −217 | 74 | 0.90 | 2 |
| Sharps | H3.4 | 14 | 22 | 289 | 1.17 1.59 | 6.08 4.50 | −199 | 133 | 0.84 | 0 |
| Parnallee | LL3.6 | 24 | −86 | 76 | 0.43 0.28 | 2.94 1.62 | −170 | 37 | 0.76 | 0 |
| Aba Panu | L3.6 | 14 | −56.2 | 49 | 1.19 0.58 | 0.46 0.24 | −71 | 71 | 0.10 | 0 |
| Tieschitz | H/L3.6 | 20 | 223 | 321 | 2.54 1.67 | 5.98 4.17 | −162 | 162 | 0.81 | 1 |
| Mezö-Madaras | L3.7 | 26 | −59 | 63 | 0.26 0.21 | 0.91 0.44 | −123 | 27 | 0.76 | 0 |
| Ceniceros | L3.7 | 10 | −145 | 61 | 0.16 0.17 | 4.08 1.18 | −158 | 34 | 0.69 | 1 |
| Bremervörde | H/L3.9 | 10 | −170 | 30 | 0.17 0.11 | 4.59 1.65 | −197 | 25 | 0.59 | 0 |

[a] N = number of SIMS analyses.
[b] Mean δD of bulk matrix, ± represents 1σ standard deviation of the mean.
[c] Mean $^{13}C/^{1}H$ and $^{1}H/^{29}Si$ of bulk matrix, ± represents 1σ standard deviation of the mean.
[d] δD value of intrinsic water for individual UOCs ≥ 3.2 as determined with D/H vs $^{13}C/^{1}H$ correlations.
[e] Pearson Correlation coefficient, where a perfect correlation between data points = 1.
[f] Number of analysis excluded from δD vs. $^{13}C/^{1}H$ fit.

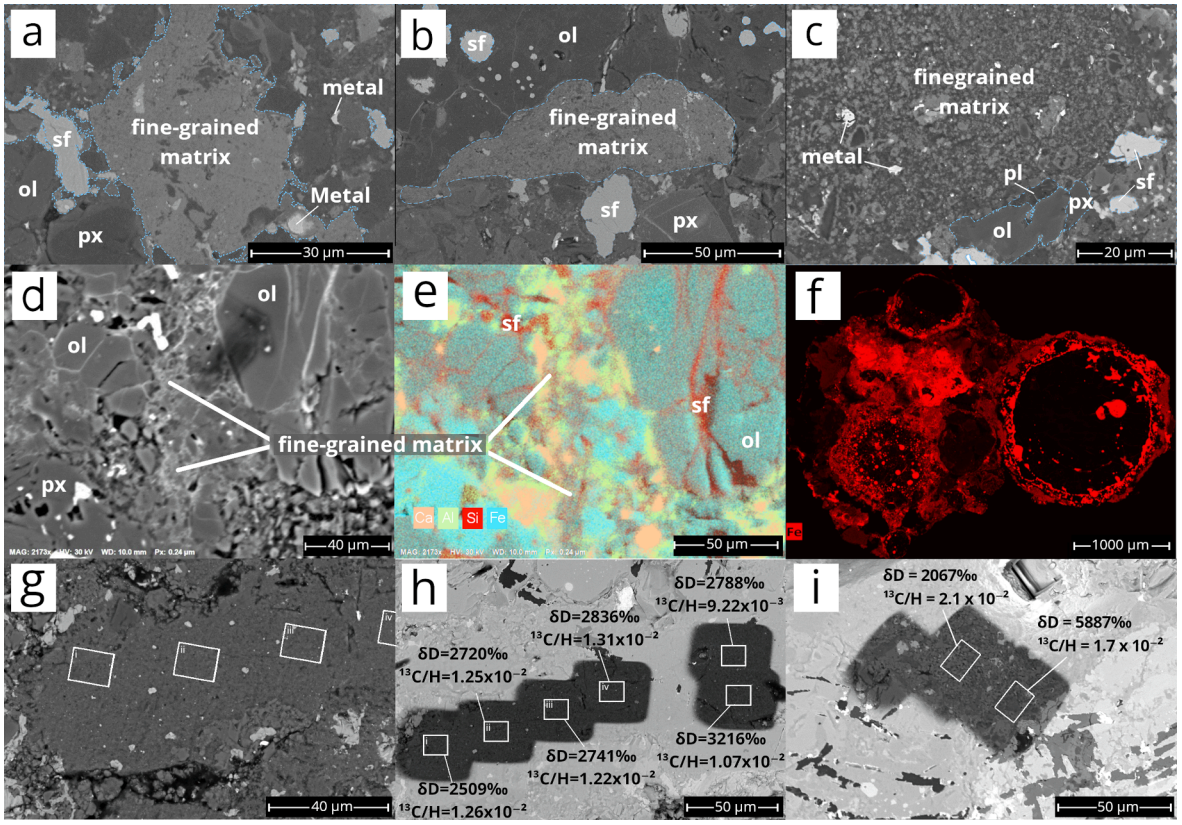


**Fig. 1.** SEM images of a variety of matrix regions in different UOCs: (a-c) BSE images of matrix in Bishunpur (LL3.15) showing differences in texture, from (a) smooth, homogeneous, and comprising of a light-grey, very fine-grained material to (b,c) matrix that is increasingly heterogeneous in grain size and texture; (d-e) BSE and EDS combined X-ray images of the same region of Bremervörde (H/L3.9) showing an area of fine-grained matrix; (f) false coloured EDS Fe X-ray map of Chainpur (LL3.4) showing that the sample is dominated by a few chondrules with Fe-rich interstitial matrix; (g-h) BSE images of the same region of matrix in Semarkona (LL3.00) before (g) and after (h) SIMS analysis, where D/H and $^{13}C/H$ ratios are given in (h); (i) BSE image following SIMS analysis of the region of Ngawi (LL3.1–3.7) matrix with the highest measured D/H ratio. Abbreviations are ol = olivine, pl = plagioclase, px = pyroxene, sf = sulfide.

Semarkona and Bishunpur matrix areas are generally consistent with literature data for Semarkona matrix (Fig. 2; Huss et al., 1981; Matsunami, 1984; Hutchison et al., 1987; Alexander et al., 1989). Overall, there is a general increase in Fe and decrease in Si abundances with increasing petrologic subtype within the LL group, except for Parnallee (Fig. 2).

EPMA analyses gave average oxide totals that ranged from ~ 83 wt% for Chainpur (LL3.4) up to ~ 98 wt% for Mezö-Madaras (L3.7) (Table 1). Totals generally increase with petrologic subtype. In the two meteorites of lowest subtype, Semarkona (LL3.00) and Bishunpur (LL3.15), there are numerous large (>100 µm across) regions of fine-grained matrix which contain micron-scale heterogeneities and are relatively porous.

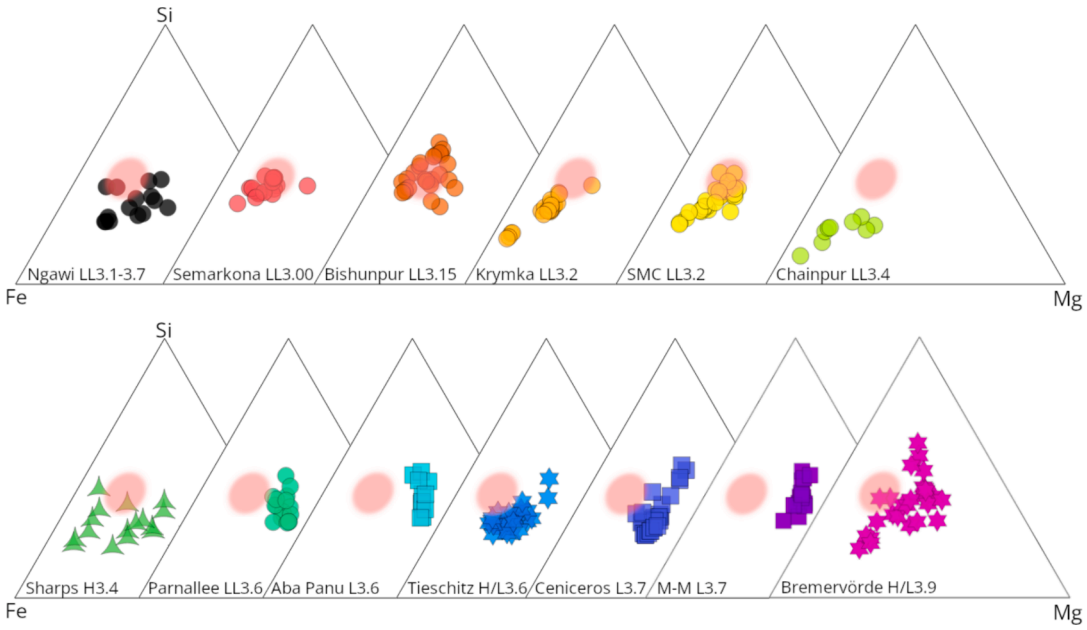


**Fig. 2.** Si-Fe-Mg ternary plots (wt%) showing individual EPMA analyses from several matrix areas for each sample, in order of increasing petrologic subtype, where symbols represent different groups (circles = LL, square = L, star = H/L, triangle = H). The red field represents the average matrix composition determined for Semarkona in previous studies (Huss et al., 1981; Matsunami, 1984; Hutchison et al., 1987; Alexander et al., 1989). SMC = St Mary's County, M−M = Mezö-Madaras.

For the least equilibrated UOCs, individual analyses have $SiO_2$ abundances ranging from ~ 30 to 49 wt%, with averages of 35.6 ± 2.4 wt% (N = 18) and 42.7 ± 3.8 wt% (N = 26) for Semarkona and Bishunpur, respectively (Table 1). For low subtype UOCs, MgO positively correlates with $SiO_2$ (Supp. Fig. S2a). There are weak positive correlations between $Na_2O$ vs. $SiO_2$ and $Al_2O_3$ vs. $SiO_2$ in some samples, such as Bishunpur, St Mary's County, Parnallee, Mezö-Madaras, and Bremervörde, while FeO is negatively correlated with $SiO_2$ (Supp. Fig. S2b-d). Matrix areas in Semarkona contain slightly more Na, Fe, Ca, and K than those in Bishunpur. Matrix areas in our Ngawi sample have similar textures to those in Semarkona and Bishunpur, but Ngawi matrix areas contain higher abundances of FeO (26.9 ± 8.5 wt% vs. ~ 20–22 wt%) and MgO (20.4 ± 6.4 wt% vs. ~ 12–13 wt%). This difference is also clear on Si-Fe-Mg ternary diagrams (Fig. 2). Ngawi matrix also has lower $Al_2O_3$, $Na_2O$, and $K_2O$ abundances than matrix areas in Semarkona and Bishunpur (Table 1).

Our mounted chip of Krymka (LL3.2) has one of the highest abundances of interchondrule matrix of all the samples studied, determined by point counting to be ~ 20 % matrix, comparable to Semarkona (~18 % matrix). Samples of higher subtypes generally contain ~ 10–15 % matrix, although chip sizes and matrix abundances are too small to provide accurate estimates of matrix abundances for bulk chondrites. The matrix in Krymka is very fine-grained, Fe-rich, and non-porous. Very few mineral fragments can be observed, with most larger grains within the matrix appearing to be chondrule fragments. Krymka matrix has relatively low $SiO_2$ (32.0 ± 4.3 wt%) and MgO (11.1 ± 3.0 wt%) abundances compared to other UOCs of low subtypes (Fig. 2). In contrast, St Mary's County (LL3.3), Chainpur (LL3.4), and Tieschitz (H/L3.6) all have very porous and heterogeneous matrix areas, with larger mineral grains than in Semarkona, Bishunpur, and Krymka.

Matrix regions in Sharps (H3.4), Parnallee (LL3.6), and Aba Panu (L3.6) tend to be quite small, <50 μm across; texturally, they are generally not very porous and are comprised of larger (~5 μm) grains. UOCs of the highest subtypes, Ceniceros (L3.7), Mezö-Madaras (L3.7), and Bremervörde (H/L3.9), have the least amount of fine-grained matrix, which consists almost entirely of thin regions between higher amounts of small (1–5 μm) silicate grains (Fig. 1e, f). The matrix in Ceniceros and Bremervörde contains numerous small (<10 μm) Fe,Ni grains and appears to be more porous than in Mezö-Madaras, as is reflected by higher EPMA totals in the latter (Table 1). Regions of truly fine-grained material (i.e. grains < 1 μm) in all three of these samples are limited and are in the range of 10′s of μm in width.

In (Mg + Fe)-Al-Si atom % ternary plots (Fig. 3), matrix compositions for most samples fall along the olivine-albite tie-line, as observed by Ikeda et al. (1981) and Matsunami (1984). Several matrix analyses also fall between olivine and the (Mg + Fe) apex for Krymka, Chainpur, Sharps, and Bremervörde as a result of high Fe contents, rather than the presence of a high-Mg phase.

### 3.2. *Matrix hydrogen isotope composition*

SIMS analyses show that UOC matrix displays significant D/H and C/H variations, both within and between meteorite samples, particularly in UOCs of lower petrologic subtypes (Figs. 4 - 5). Overall, average δD values of matrix analyses range from −170 ± 30 ‰ for Bremervörde (H/L3.9), the UOC with the highest petrologic subtype in our sample set, to +2230 ± 1140 ‰ for Semarkona (LL3.00), the sample with the lowest petrologic subtype (Table 2). Semarkona, Ngawi, and Bishunpur have the largest spreads of D/H ratios, with δD values ranging between *ca.* −250 and +6000 ‰ (Fig. 4) and standard deviations of the mean δD > 1000 ‰ in all three samples, with the highest D/H ratio measured in Ngawi (LL3.1–3.7 breccia). In general, the average matrix δD values and their heterogeneity decrease with increasing petrologic subtype, with the exception of Tieschitz (H/L3.6) which displays a large spread of δD values compared with other UOCs of the same subtype (Fig. 4).

The analysed areas in UOC matrix likely include some H from C-rich organics. We can assess the contribution of organics in a D/H vs. $^{13}C/H$ plot, in which one would expect multiple analyses in a given sample to trend toward a C-rich organic end-member, as observed for *in situ* SIMS analyses in most carbonaceous chondrites (e.g., Piani et al., 2018, 2021; Piani and Marrocchi, 2018). In such diagrams, the $^{13}C$-free y-axis intercept is generally interpreted as corresponding to the D/H of the water accreted by the meteorite parent asteroid. In the UOCs we studied, we observed rough positive linear correlations between δD vs. $^{13}C/H$ for all samples with subtypes ≥ 3.2 (Fig. 6, Supp. Fig. S3). These linear regressions appear as curves in the D/H vs. $^{13}C/H$ plot of Fig. 5, where

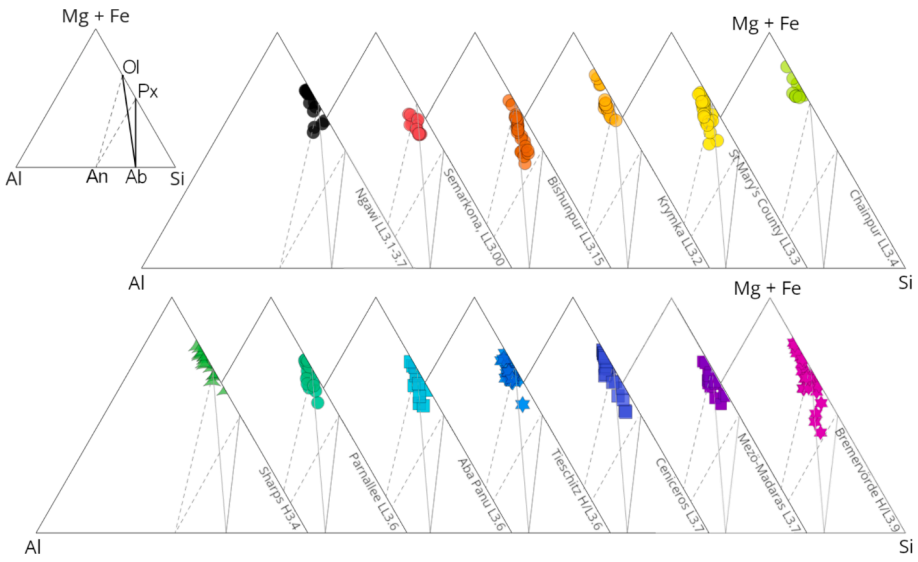


**Fig. 3.** (Mg + Fe)-Al-Si ternary plots (at%) showing individual EPMA analyses from several matrix areas for each sample, in order of increasing petrologic subtype. Solid lines represent tie-lines between olivine (Ol), pyroxene (Px), and albite (Ab) compositions, and dashed lines represent the tie-lines between olivine, pyroxene, and anorthite (An) (see inset).

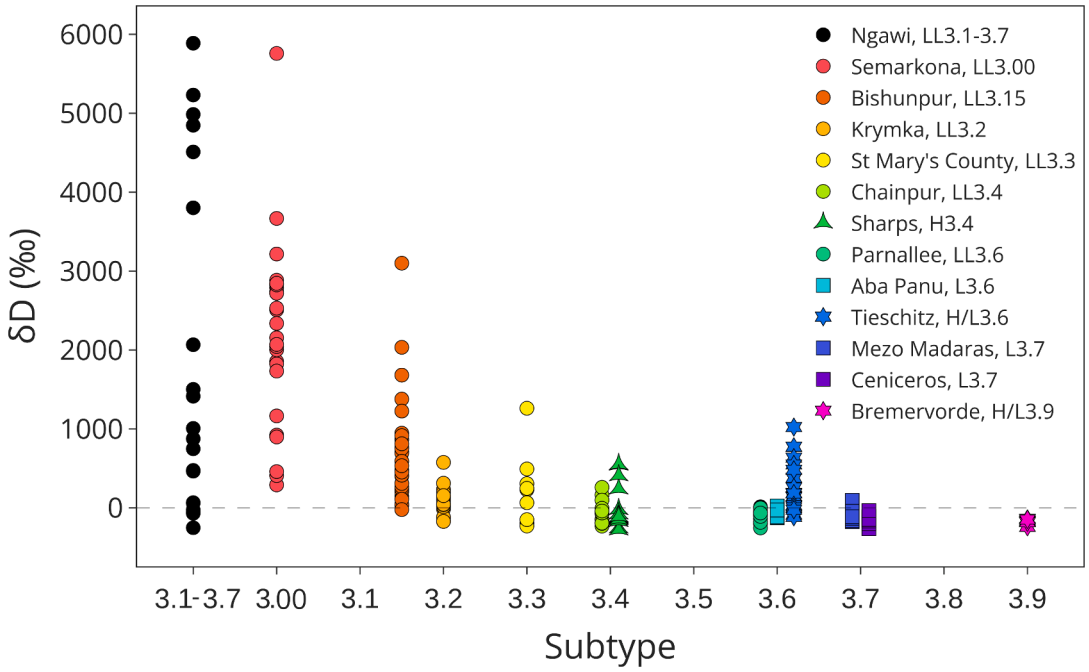


**Fig. 4.** Matrix δD values in individual SIMS analyses vs. petrologic subtype (samples with the same subtypes offset for clarity).

$^{13}C/H$ is plotted on a logarithmic scale on the x-axis. The mixing lines shown in Figs. 5 and 6 have end-members consistent with water (y-axis intercept) and an insoluble organic matter (IOM) component akin to that found in the L3.2 meteorite GRO 95502 for all samples but Aba Panu (for which there is a weak, flat, correlation between D/H and $^{13}C/H$). The D/H vs. $^{13}C/H$ correlations for Krymka (LL3.2) and Chainpur (LL3.4) are steeper than in other samples (Fig. 6), suggesting a slightly higher D/H for their organic-rich end-member. Linear regressions between δD and $^{13}C/H$ for samples with subtypes ≥ 3.2 yield intrinsic water $(\delta D)_i$ values between −320 ± 91 ‰ and −71 ± 71 ‰, with most calculated water $(\delta D)_i$ values being between ca. −200 and −100 ‰ (Table 2 and Supp. Fig. S3).

Matrix analyses in Ngawi, Semarkona, and Bishunpur do not display a similar, simple two-component mixing behaviour (Figs. 5, 7). Instead, they appear to fall in a triangle between (i) a C-poor / low δD pole akin to the composition estimated for water in subtypes ≥ 3.2, (ii) a C-rich / intermediate δD pole akin the composition of UOC IOM, and (iii) a pole with intermediate $^{13}C/H$ ratios (~0.01–0.02) and very high δD values up to 6,000 ‰ which we describe as a "D-rich unknown phase". In Fig. 7, which shows only analyses for these three chondrites, $^{13}C/H$ is plotted on a linear scale. The C-poor phase is labelled as phyllosilicate in Figs. 5 and 7: phyllosilicates are hydrated silicates which are likely the main carriers of water in UOC matrices.

Because average $SiO_2$ abundances for matrix areas across the whole sample set are fairly consistent (Table 1), measured $^{1}H/^{29}Si$ ratios provide a qualitative estimate for matrix $H_2O$ abundances. Matrix areas in the least metamorphosed samples Semarkona and Bishunpur have average $^{1}H/^{29}Si > 10$, while samples with subtypes ≥ 3.6 have average

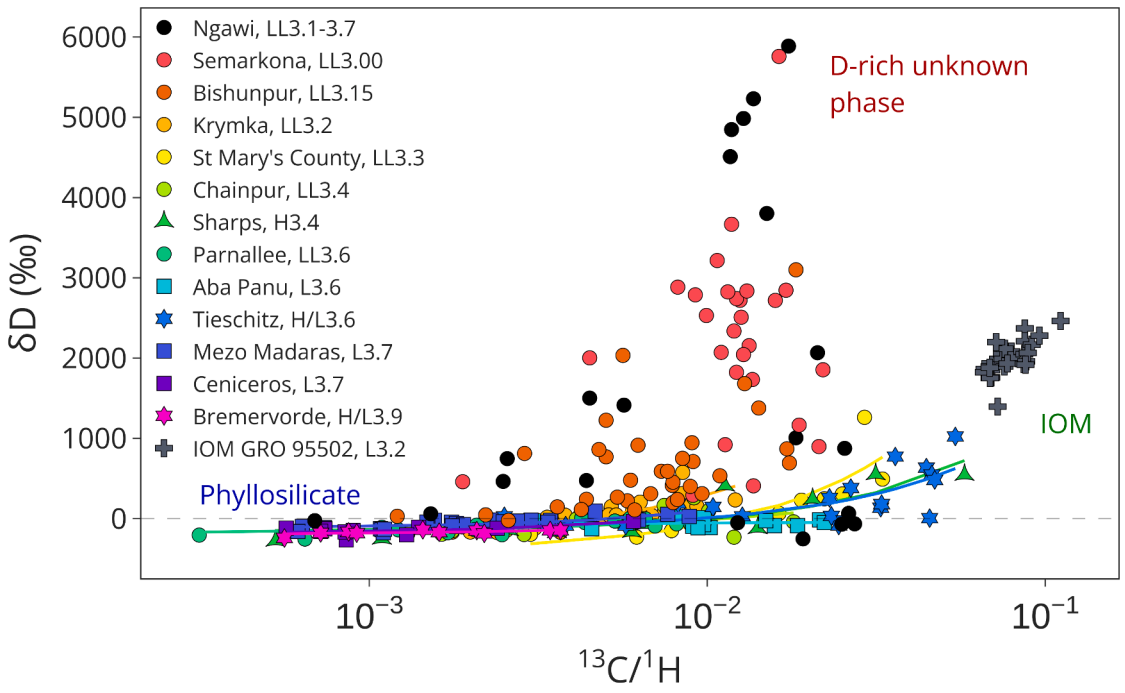


**Fig. 5.** δD vs. $^{13}C/H$ for UOC matrix analyses, as well as insoluble organic matter from the L3.2 meteorite GRO 95502. Coloured lines are linear regressions for petrologic subtypes ≥ 3.2. The grey dashed line at δD = 0 ‰ represents the Earth ocean mean δD value.

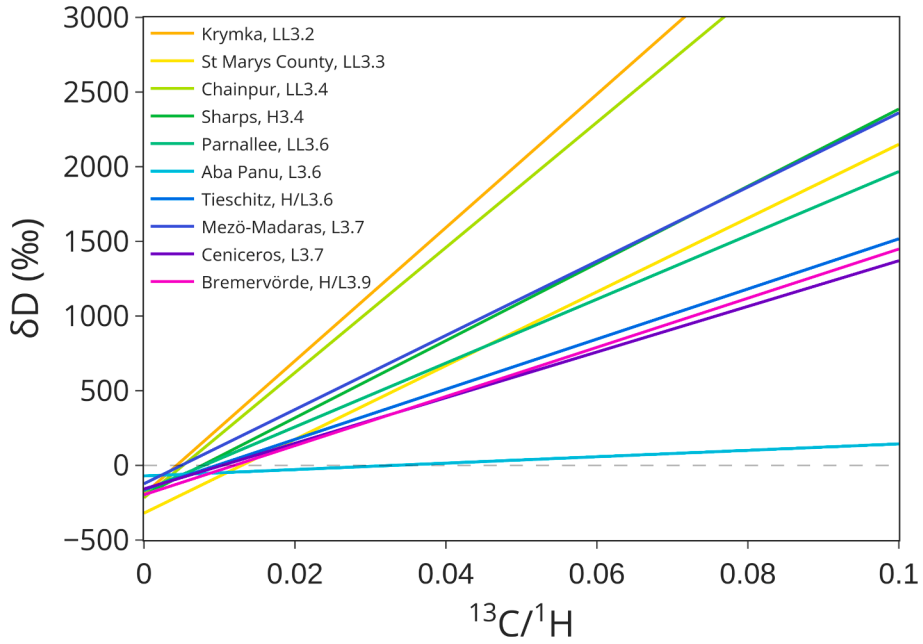


**Fig. 6.** $(\delta D)_i$ vs. $^{13}C/H$ linear regressions for matrix analyses of UOCs ≥ 3.2. Values at $^{13}C/H = 0$ (i.e. the y-intercept) are δD water as given in Table 2. The grey dashed line represents the Earth ocean mean δD value.

$^{1}H/^{29}Si$ < *ca.* 5 (Table 2), which is consistent with lower matrix $H_2O$ abundances in the more metamorphosed samples. To a first order, Fig. 8 also shows that the spread of matrix $^{1}H/^{29}Si$ ratios tends to decrease with increasing subtype. Chainpur (LL3.4) displays a few analyses with much higher $^{1}H/^{29}Si$ compared to other samples; as H count rates in these analyses are similar to H count rates in other low subtype UOCs, these elevated $^{1}H/^{29}Si$ values are likely caused by low Si abundances.

## 4. Discussion

Our goal in this study is to identify the source of high D/H ratios measured in bulk UOCs (Robert et al., 1979, 1987; McNaughton et al., 1981, 1982; Yang and Epstein, 1983; Alexander et al., 2012; Grant et al., 2023), using the same meteorites as those analysed by Grant et al. (2023). In the following discussion, we first evaluate our bulk matrix compositions as determined by EPMA, in order to understand any chemical differences that might accompany isotopic trends. Following this, we divide the discussion of our SIMS dataset into two groups: 1)

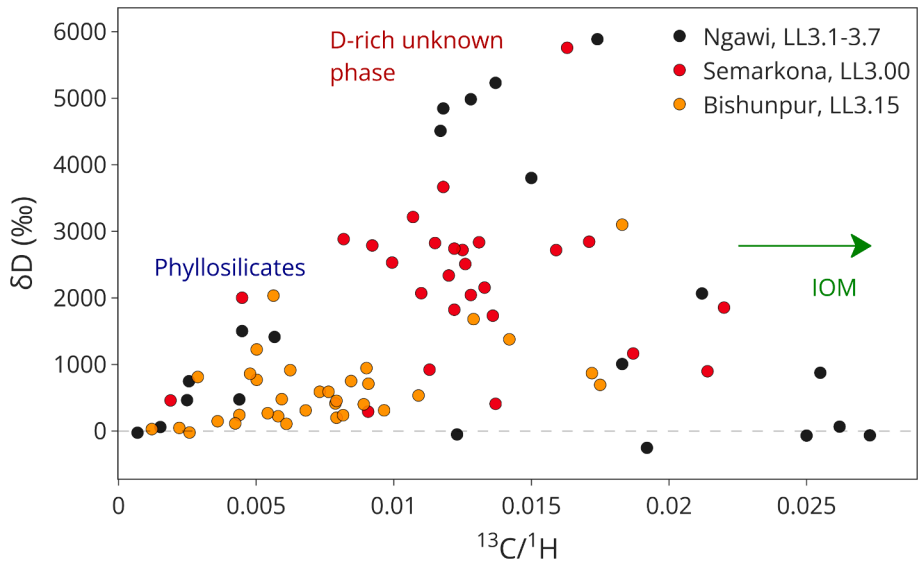


**Fig. 7.** δD vs $^{13}C/H$ for Ngawi (LL3.1–3.7), Semarkona (LL3.00), and Bishunpur (LL3.15). Data from these samples plot in a roughly triangular space with end members of UOC water (labelled phyllosilicates), UOC IOM, and a D-rich unknown phase. The grey dashed line at δD = 0 ‰ represents the Earth ocean mean δD value.

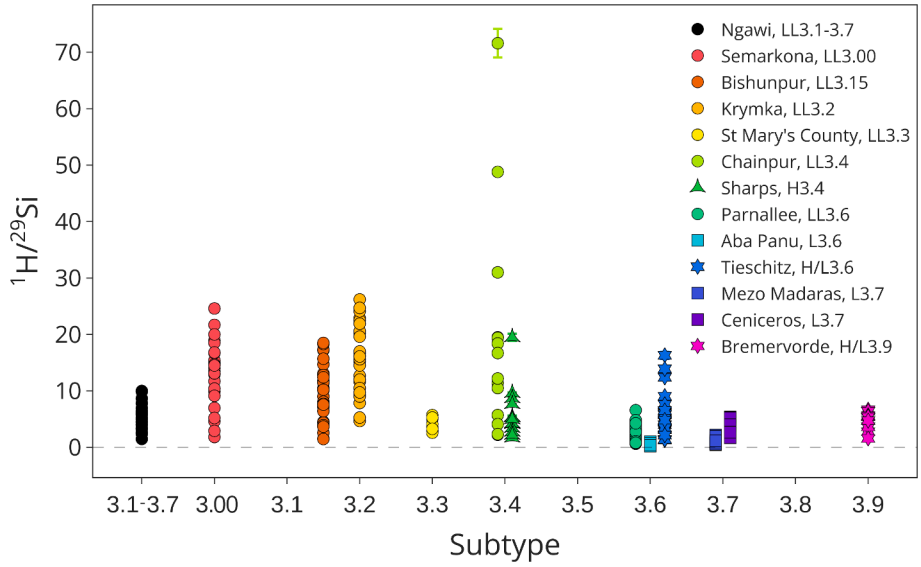


**Fig. 8.** Measured matrix $^{1}H/^{29}Si$ ratios. Error bars represent 1σ uncertainties for each individual area across 30 cycles.

higher subtype UOCs which show linear correlations between $^{13}C/H$ and D/H, and which help determine intrinsic water D/H ratios, and 2) the three lowest subtype UOCs, which contain the highest D/H ratios and in which data do not define a linear trend, suggesting a third, unidentified carrier of high D/H in UOCs. We discuss the possible nature and origin of this high D/H component, and the mechanisms by which it became incorporated into OC parent bodies.

### 4.1. Matrix compositions of type 3 ordinary chondrites

Comparison with existing literature on the chemical composition of the matrices of UOCs selected for this study allows for the assessment of whether target matrix regions in our set of samples are typical and, therefore, reliable for interpreting SIMS analyses. Any regions whose composition did not agree with existing literature were presumed to be either not matrix or at least non-representative of most fine-grained interstitial matrix and therefore excluded from future analyses. In addition, an understanding of the chemical composition of the matrix can help with isotopic interpretation and to explain any unusual isotopic compositions. Generally, our measured bulk compositions of matrix are in good agreement with literature data. For example, Fig. 9 shows that the bulk matrix elemental composition we measured for Semarkona, considering heterogeneities across different matrix areas, is consistent with literature data for major elements (Huss et al., 1981; Matsunami, 1984; Hutchison et al., 1987; Alexander et al., 1989).

The average major element oxide totals for all samples with petrologic subtypes lower than 3.6 are < 95 wt%. This is due to the porosity of fine-grained matrix, as observed with SEM, as well as the contribution of hydrated phyllosilicates with an OH component, and C-rich organic phases, which cannot be detected with EPMA. Oxide totals tend to increase with increasing petrologic type, consistent with an overall decrease in porosity and in the abundance of hydrated and/or organic-rich material in the matrix with increasing thermal metamorphism. A decrease in the abundance of hydrated material is consistent with

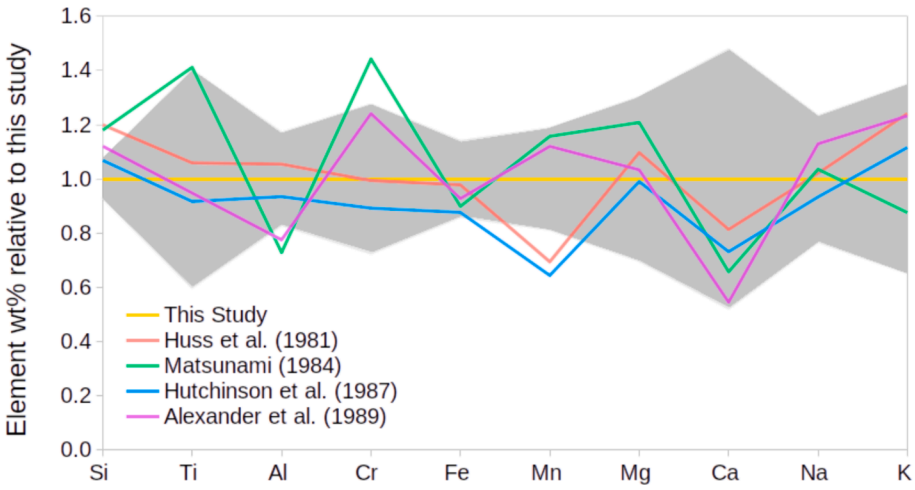


**Fig. 9.** Comparison of our Semarkona bulk matrix major element composition with data reported in the literature. Alexander et al., (1989) did not report Ti. The grey band represents one standard deviation on the mean EPMA values within our Semarkona dataset.

observations of decreasing bulk UOC $H_2O$ content with increasing petrologic type in the same set of UOCs (Grant et al., 2023).

Due to the complex nature of matrix, it is not possible to identify the mineralogy from EPMA data alone. Nevertheless, it is possible to draw some conclusions about the variability within and between samples. Fig. 3 shows matrix analyses in each of the samples plotted on (Mg + Fe) – Al – Si ternary plots where the positions for olivine, pyroxene, and plagioclase are represented. As expected, most samples plot on or around the olivine/pyroxene tie-line, due to the dominance of these anhydrous silicates in OC matrix (e.g. Alexander et al., 1989). Analyses in some samples such as Bishunpur and Bremervörde show a spread along the olivine/albite tie-line, in agreement with previous observations of albite-rich amorphous "glue" in the matrix of Bishunpur (Alexander et al., 1989).

Overall, there is a decrease in S contents in matrix with increasing petrologic subtype (Table 1), a trend that has previously been identified in UOCs (e.g., Grossman and Brearley, 2005). This occurs because fine-grained sulfides are abundant in the matrices of the least metamorphosed UOCs, but as UOCs undergo progressive thermal metamorphism, FeS grains coarsen out of the fine-grained matrix and, therefore, their contribution to bulk fine-grained matrix chemistry decreases (Grossman & Brearley, 2005).

Except for a few discrepancies in minor element abundances such as K, Cr, and Mn, we find that bulk matrix chemical compositions for most samples compare within errors with previously measured compositions of the same UOCs (matrix compositions have been reported for all the studied UOCs except St Mary's County, Aba Panu, and Ceniceros; Huss et al., 1981; Matsunami, 1984; Alexander et al., 1989; Grossman and Brearley, 2005). However, there are some significant differences for a few samples, notably Chainpur. While it is not unusual for the matrix in Chainpur to be depleted in $SiO_2$ and enriched in FeO relative to other UOCs (Huss et al., 1981; Matsunami, 1984; Alexander et al., 1989), as can be observed in Figs. 2 and 3, we nevertheless find our sample of Chainpur to be more divergent than in these previous studies. Our average matrix composition for Chainpur is depleted in $SiO_2$ (26.8 wt% (normalised to 100%) vs. 36.5 to 45.2 wt%) and enriched in FeO (49.6 wt% (normalised) vs. 29.3 to 38.0 wt%) compared with Huss et al. (1981), Matsunami (1984) and Alexander et al. (1989). We also find Chainpur to be depleted in Na and Al relative to previous studies, and it has the lowest oxide total at ~ 83%. One possible explanation could be issues with data acquisition for Chainpur, for example charging due to uneven sample topography, although errors are similar to those of other measurements. Alternatively, it is possible that the region of Chainpur we are measuring is intrinsically different to those previously analysed. Our Chainpur sample is one of the smallest we analysed at only ~ 5 $mm^2$, a significant portion of which is dominated by a large (~2 $mm^2$) chondrule (Fig. 1f). Due to the heterogeneity of Chainpur (Huss et al., 1981; Matsunami, 1984; Alexander et al., 1989), and the small size of the sample, it is possible that we are simply sampling an Si-poor, Fe-rich region of matrix. Furthermore, Fig. 8 shows that the $^1H/^{29}Si$ abundance in a few analyses of these same matrix areas is unusually high relative to matrix analyses in other samples, which we interpret to be due to a low Si content, rather than a high H content.

Tieschitz has previously been described as having two distinct types of matrices, so-called white matrix which is a vein-like Na-, K-, and Al-rich intergrowth of multiple phases dominated by albitic plagioclase, and an FeO-rich black matrix which commonly surrounds the white matrix (Christophe-Michel-Lévy, 1975; Dobrică & Brearley, 2014). In our study, all reported EPMA points were on black matrix. We find the average composition of black matrix in Tieschitz to be low in $SiO_2$ (32.9 wt%), $Na_2O$ (1.1 wt%), and $Al_2O_3$ (2.6 wt%) relative to other UOCs, with an FeO content of 26.0 wt% (EPMA total of 88.3 wt%) (Table 1). These values are in close agreement with previous measurements of black matrix in Tieschitz (Christophe-Michel-Lévy, 1975; Huss et al., 1981; Matsunami, 1984, Dobrică & Brearley, 2014).

### 4.2. *D/H ratios of matrix in UOCs with petrologic subtypes ≥ 3.2*

All samples of subtypes ≥ 3.2 (excluding Ngawi, a breccia which we discuss below) show a range of matrix δD values spanning between *ca.* −275 and + 1250 ‰; Fig. 4). Calculated water-specific $(\delta D)_i$ values, however, show relatively little variation (Table 2, Supp. Fig. S3). Figs. 5–6 and Supp. Fig. S3 show that matrix in UOCs of petrologic subtypes ≥ 3.2 display linear arrays between (1) C-bearing organic material with D/H ratios of up to δD ~ 1000–2000 ‰, similar to that of IOM previously measured in UOCs (Alexander et al., 2007; Piani et al., 2015; Remusat et al., 2016), and (2) C-free, relatively D-poor (δD between −320 ± 91 ‰ and −71 ± 71 ‰) material (the water-specific component). The mineralogical nature of this H bearing phase remains to be conclusively determined. One possibility is minor amounts of hydrated phases, such as phyllosilicates, residual in the matrix following incipient thermal metamorphism. Phyllosilicates are the dominant water host in UOC matrices of the lowest subtypes (e.g. Alexander et al., 1989) and bulk water abundances for UOCs with subtypes ≥ 3.2, albeit small, are non-zero (Yang and Epstein, 1983; Vacher et al., 2020; Grant et al., 2023). To our knowledge, phyllosilicates have not been observed in the matrix of UOCs with subtypes ≥ 3.2. However, Eschrig et al. (2021) analysed a large set of UOCs with subtypes ranging from 3.0 to >

3.6 using reflectance spectroscopy and showed that all these samples exhibit well developed 3 μm hydration bands, with levels of hydration higher than for CV and CO chondrites. It is possible that the presence of H-bearing phases in the matrix of UOCs with subtypes ≥ 3.2 are, in part, a result of terrestrial contamination. However, we find this unlikely as all the meteorites studied here are falls that have been stored under similar conditions, and yet matrix H abundances are not consistent across UOCs with subtypes ≥ 3.2, as would be expected if all of the H-bearing component were a result of terrestrial contamination. In fact, similarly to bulk studies, we find indications that matrix H abundances decrease with increasing thermal metamorphism, suggesting an inherited water content that is progressively lost with thermal metamorphism. Another possibility is the presence of H-bearing nominally anhydrous minerals (NAMs) such as olivine and pyroxene. For example, the latter may contain a few hundred parts per million $H_2O$ in types 5 and 6 OC falls, with δD values of *ca.* −250 ± 50 ‰ (Jin et al., 2021), which is comparable to the $(\delta D)_i$ values measured in the matrix of many of the studied UOCs. Ultimately, we cannot be certain what the H-bearing phase is in the matrix of these UOCs with subtypes ≥ 3.2, as high-resolution mineralogical studies of the fine-grained matrix in these meteorites are lacking.

Tieschitz matrix is enriched in C compared with other UOCs with subtypes ≥ 3.2, as indicated by generally higher $^{13}C/^{1}H$ ratios (Fig. 5), which suggests a higher abundance of organic material. Therefore, the relatively high D/H ratios we measured in Tieschitz matrix, in comparison to other UOCs of comparable petrologic subtype (Fig. 4, Table 2), likely relate to higher abundances of D-rich organics. This may also explain the higher bulk D/H measured for Tieschitz compared to other UOCs with similar petrologic subtypes (Grant et al., 2023).

Overall, there does not appear to be any trend between intrinsic water D/H ratio and UOC petrologic subtype, similar to observations made for CCs (Piani et al., 2021). For UOCs with subtypes ≥ 3.2, we find that the intrinsic water D/H ratios (δD of *ca.* −320 to −70 ‰) are consistent with δD values of *ca.* −200 ‰ measured in NAMs in the primitive achondrite groups, acapulcoites and lodranites, which are believed to have formed from OC-like precursors (Stephant et al., 2023). These UOC intrinsic water D/H ratios are also similar to those of CV and CM chondrites, which have $\delta D_{water}$ between *ca.* −350 ‰ and −77 ‰, respectively (Piani & Marrocchi, 2018). This indicates that UOCs, and therefore OC parent bodies, likely accreted water/ice with similar D/H ratios to that of some carbonaceous chondrites, and notably CMs and CVs. This important observation alleviates the apparent issue associated with bulk H isotope studies of UOC that seemed to indicate that UOC parent bodies accreted water ice with higher D/H ratios than parent bodies of some CC types that formed much further out in the protoplanetary disc (e.g., Yang et al., 2013; Jacquet and Robert, 2013; Piani et al., 2021; Grant et al., 2023). Indeed, the fact that parent bodies of UOCs of subtype ≥ 3.2 (i.e. the inner Solar System population) appear to have accreted water ice with similar δD to that of the CC parent bodies (i.e. the outer Solar System population) may suggest that this isotopic water composition corresponds to the background early Solar System H isotope composition in the chondrite parent asteroid formation region. This background can be established through isotopic exchange between water vapour, produced by the sublimation of D-rich ice, and protosolar $H_2$ gas (Geiss and Reeves, 1981).

### 4.3. D/H ratios of matrix in Semarkona, Bishunpur, and Ngawi

The UOCs of the lowest petrologic subtypes, Semarkona (LL3.00) and Bishunpur (LL3.15), display a different distribution of D/H vs. $^{13}C/^{1}H$ ratios compared with UOCs of subtypes ≥ 3.2 (Figs. 5 and 7). As discussed above, Ngawi is a breccia that samples two distinct lithologies, LL3.1 and 3.7 (Sears et al., 1991; Grossman and Brearley, 2005). Here we treat our Ngawi sample as subtype LL3.1, due to its unusual isotopic distribution that is comparable to that of Semarkona and Bishunpur, and we discuss these three samples together. The highest δD values (up to 6000 ‰) measured in Semarkona and Ngawi are significantly higher than their bulk δD contents and, when considering the relatively large size of SIMS points relative to NanoSIMS, are comparable to some of the highest δD values previously measured in the matrix of Semarkona (+10,600 ‰) using NanoSIMS by Piani et al. (2015). In addition, the presented D/H ratios represent lower limits following calibration. Where UOCs of higher subtypes show broadly linear correlations between the D/H and $^{13}C/^{1}H$ ratios, which we interpret as a two-component mixing array between hydrated and organic materials, these three low subtype samples instead show an apparent three-component distribution (Figs. 5 and 7). This suggests that hydrogen, and thus deuterium, is dominantly hosted in the matrix of these samples by a mixture of (i) an organic component with moderate D/H, (ii) relatively D-poor hydrated minerals (likely phyllosilicates), and (iii) a third phase which is C-bearing (i.e. non-zero C/H, but with a lower C/H ratio than the organic material) and extremely D-rich (δD > 3000 ‰).

Previously, high D/H ratios (>1000 ‰) have been reported in all three of these samples both via bulk analyses (e.g., Robert et al., 1979; McNaughton et al., 1981, 1982; Yang and Epstein, 1983; Alexander et al., 2012; Grant et al., 2023) and *in situ* measurements (e.g., Deloule and Robert, 1995; Alexander et al., 2010; Piani et al., 2015; Remusat et al., 2016). In the case of bulk data, chondrules and other high temperature nebular components are unlikely to contribute much to the measured values, although they have been shown to contain minor amounts of H (Robert et al., 1987; Stephant et al., 2017). Previous *in situ* studies have focused specifically on deuterium-rich 'hotspots' found within either hydrated material (Piani et al., 2015) or IOM (Alexander et al., 2010; Remusat et al., 2016). While we certainly find evidence for the presence of moderately D-rich organic material, similar to previous *in situ* studies (Figs. 5 and 7), this organic component is by no means the most D-rich phase found in low subtype UOCs. Also, we find no evidence of a high D/H and low C/H component, as would be expected if hydrated material were the dominant host of deuterium in the matrix of these samples. As discussed above, all UOC samples analysed here, which cover the whole type 3 range, consistently point to a D-poor water ice component accreted to their parent body, similar to that accreted to the parent asteroids of most CC types.

A number of conflicting mechanisms have been proposed to explain the unusually high D/H ratios found in the least metamorphosed UOCs. For example, Alexander et al., (2007,2010) have suggested that degassing of $H_2$ produced by iron oxidation in a hydrated parent body preferentially leaves behind D-rich material that would generate bulk D enrichments with increased heating and oxidation intensity. However, this model would imply that moderately metamorphosed UOCs (i.e. subtypes ~ 3.2–3.4) should exhibit the highest bulk D/H ratios, which does not agree with our bulk UOC D/H analyses in which the highest D/H ratios are observed in subtypes < 3.2 (e.g., Grant et al., 2023). Bulk D/H ratios in UOCs globally decrease with progressive water loss and increasing petrologic subtype (Grant et al., 2023), suggesting that the D-rich material(s) is susceptible to breakdown during thermal metamorphism. Thus, it is more likely an inherited component from the molecular cloud and/or protoplanetary disc processes (e.g., Grant et al., 2023), as has been proposed recently for CM chondrites (Marrocchi et al., 2023). Furthermore, the complete absence of this elusive D-rich phase in the matrix of UOCs with subtypes ≥ 3.2, and indeed its relative scarcity even in Bishunpur, suggests that this phase is extremely sensitive to even mild thermal metamorphism. In contrast, IOM with a moderately high D/H ratio is comparatively thermally resistant (e.g., Remusat et al., 2016) and cannot account for these matrix observations.

One possible candidate for the extremely D-rich phase may be primitive amorphous silicates, which have been identified via high-resolution transmission electron microscopy (HRTEM) in Semarkona (LL3.00) and MET 00526 (LL3.05) (Dobrică & Brearley, 2020a, 2020b; Zanetta et al., 2022), and which has also been observed in a limited number of pristine carbonaceous chondrites (e.g., Abreu and Brearley, 2010; Brearley, 1993; Le Guillou and Brearley, 2014; Zanetta et al.,

2022). These amorphous silicates are very sensitive to both thermal and aqueous alteration. The observation that they occur extensively in the matrix of Semarkona, in regions of matrix that do not contain phyllosilicates, suggests that post-accretion parent body aqueous alteration occurred heterogeneously, at least in this chondrite, due to a variety of factors including oxidising conditions and low water-to-rock ratios (Dobrică and Brearley, 2020a). Alternatively, pre-hydration of matrix phases could have occurred in the protoplanetary disc, as has been proposed for carbonaceous chondrites (Marrocchi et al., 2023). The amorphous material is probably a residual component from the early protoplanetary disc that has undergone no metamorphism following parent body accretion (Le Guillou and Brearley, 2014). There are a number of hypotheses for the origin of primitive amorphous material in the protoplanetary disc, with varying levels of applicability to the high δD material found in this study. For example, a great deal of amorphous silicates in the universe are produced in the envelopes of late-type AGB stars and type II supernovae, however these silicates are expected to be essentially devoid of deuterium (e.g. Matsuura et al., 2011; Weinberg, 2017; Höfner and Olofsson, 2018). A more likely source is one of 'local origin', for example by direct condensation out of the gas in the cold molecular cloud or thermal processing in the protosolar nebula (Abreu and Brearley, 2010; Nittler and Ciesla, 2016; Dobrică and Brearley, 2020a; Zanetta et al., 2022).

In their study of the CR chondrites Queen Alexandra Range (QUE) 99,177 and Meteorite Hills 00426, Le Guillou et al. (2015) estimated that the amorphous silicates have $H_2O$ abundances of ~ 8 ± 5 wt%. Similarly, Zanetta et al. (2022) found amorphous silicate $H_2O$ abundances of ~ 4–6 ± 1 wt% in QUE 99177 and Semarkona. These amorphous silicate $H_2O$ abundances are intermediate between those of anhydrous silicates and matrix phyllosilicates (e.g., *ca.* 10 wt% $H_2O$ in bulk CI chondrites; Vacher et al., 2020), which is consistent with the intermediate $^{13}C/^{1}H$ ratios of matrix analyses with the highest δD in Semarkona and Ngawi (Figs. 5 and 7). Additionally, amorphous material in Semarkona contains embedded nanoscale carbides (Dobrică and Brearley, 2020a), which may also explain the intermediate $^{13}C/^{1}H$ ratios of Semarkona, Bishunpur, and Ngawi matrix analyses with the highest δD values.

Matrix areas of Semarkona, Bishunpur, and Ngawi with the highest D/H ratios are heterogeneous regions of fine-grained matrix (Fig. 1g-i), but there is no apparent trend between matrix texture and D/H ratio among these three samples, at the micrometer scale of SEM observations. Dobrică and Brearley (2020a) found amorphous silicates in Semarkona alongside newly forming phyllosilicates, suggesting that the latter hydrated minerals crystallised out of the amorphous material. A similar association has been observed in CM chondrites (Leroux et al., 2015). Due to the extremely fine-grained nature and heterogeneity of the phyllosilicate-amorphous silicate mixture, it is possible that previous observations of D-rich hydrated material in the matrix of Semarkona (Piani et al., 2015) included amorphous material. The cold molecular cloud and interstellar medium are known to be D-rich, with water ice D/H ratios of *ca.* 0.001–0.01 (δD = 5,420–63,000 ‰; Ceccarelli et al., 2014; Hallis, 2017), meaning that even a minor residual contribution from unmodified pre-accretionary material would be sufficient to account for the observed D/H ratios measured in the matrix of the least metamorphosed UOCs. Our interpretation that links very high δD values to the presence of primitive amorphous silicates in the matrix of Ngawi and Bishunpur could be investigated with high resolution TEM and NanoSIMS studies.

### 4.4. *Implications for understanding water reservoirs in the early Solar System*

Studies of UOCs show that the parent bodies of these meteorites accreted some water at the time of their formation (e.g., Sears et al., 1995; Alexander et al., 2010; Marrocchi et al., 2020; Vacher et al., 2020; Grant et al., 2023). Recent studies have also shown that other inner SS bodies likely accreted non-negligible amounts of water, such as the parent bodies of enstatite chondrites (Piani et al., 2020), a range of achondrites (e.g., McCubbin et al., 2021; Deligny et al., 2021; Stephant et al., 2023), NAMs in OC falls (Jin et al., 2021), and samples returned from the S-type asteroid Itokawa (Jin and Bose, 2019; Che and Zega, 2023). Furthermore, observations with the Spitzer and James Webb Space Telescopes have found evidence of water vapour reservoirs in the inner regions of protoplanetary discs, suggesting it is more common than previously thought (Carr and Najita, 2008; Perotti et al., 2023; Salyk et al., 2008). In the last decade, chondrite parent asteroids have been separated into two distinct populations based on their oxygen and nucleosynthetic isotope compositions, resulting in the so-called isotope dichotomy which presumably reflects their different formation locations in the protoplanetary disc. The non-carbonaceous (NC) population formed in the inner SS (i.e. within Jupiter's orbit) and includes ordinary and enstatite chondrite parent bodies, whereas the carbonaceous (CC) chondrites likely formed beyond Jupiter's orbit before being scattered inwards into the asteroid belt (Warren, 2011a, 2011b; Budde et al., 2016; Kruijer et al., 2017; Scott et al., 2018; Kleine et al., 2020). This dichotomy does not, however, appear to exist for hydrogen. In fact, our data show that the D/H ratios of water ice accreted by UOC and water-rich CC parent bodies are essentially the same, which we propose is indicative of a shared water, or at least hydrogen, source throughout a large region of the protoplanetary disc.

It has been suggested that the delivery of water to the inner Solar System may be a result of giant planet formation destabilising ice-rich outer SS material and scattering it into the inner SS, in the first million years after protoplanetary disc formation (McCubbin and Barnes, 2019; Raymond and Izidoro, 2017). We can consider whether this scattering might be responsible for the observed common H isotope source of inner and outer disc material. However, it is unlikely that ice alone would accrete to NC planetesimals as a result of this process, and accretion of rocky material from CC planetesimals to NC bodies would tend to erase the clear isotopic dichotomy between the two reservoirs. We therefore find the scenario of two distinct water reservoirs that undergo subsequent mixing unlikely.

We propose that the D/H ratio measured for water in OCs and CCs is representative of a common H isotope composition that spanned the formation regions of both populations. This contrasts with the current idea that water D/H ratio increases heliocentrically (e.g. Drouart et al., 1999; Alexander et al., 2012; Jacquet and Robert, 2013; Yang et al., 2013). The snow line (the region beyond which water is stable as ice) is known to have moved over the lifetime of the protoplanetary disc, and various models have predicted that it was as close as 1–1.5 AU from the Sun in the first few million years (Sasselov and Lecar, 2000; Dodson-Robinson et al., 2009). Considering the presence of water in OCs, it is likely that the OC parent bodies were outside the snow line at the time of formation (Alexander et al., 2018; Bermingham et al., 2020). OC parent bodies were therefore able to accrete water ice isotopically similar to that of CCs, despite the separation caused by Jupiter.

## 5. Conclusion

We have measured the major element composition, and H isotopic composition, of the matrices of a range of UOCs from different groups and petrologic subtypes. We find matrix chemical compositions to be generally in agreement with previous studies, confirming that our measurements of isotopic compositions are made in typical matrix areas. In UOCs with subtypes ≥ 3.2, we observe two-component mixing of hydrogen isotopes between moderately D-rich IOM and D-poor water. Correlations between D/H and $^{13}C/H$ allow for the determination of intrinsic water D/H ratios: we find $(\delta D)_i$ values between −320 ± 91 ‰ and −71 ± 71 ‰, which is similar to that of water in CM and CV chondrites (Piani and Marrocchi, 2018). We see no variation between the D/H ratio of water and petrologic subtype, therefore suggesting water D/H ratios in UOCs are inherited from the time of formation, and

are not a result of parent body processing. In the matrix of UOCs of subtype < 3.2, we observe three-component mixing between D-poor phyllosilicates, moderately D-rich organics, and a third extremely D-rich component that has low C content. We propose that all OCs accreted water ices similar to those of CC parent bodies, with δD values around −350 ‰ to 0 ‰. This alleviates the problems with water transport models in the early Solar System, where previously it was thought that OC parent bodies in the inner Solar System accreted ices isotopically similar to that of outer Solar System comets whereas CC parent bodies accreted ices originating in the outer disc region, beyond Jupiter. A possible explanation for the similar hydrogen isotope compositions of water in the NC and CC isotopic reservoirs is that the observed water D/H ratio is representative of a common hydrogen isotope composition that was homogeneous across the inner and outer Solar System during parent body formation, and that the snow line was inwards of the asteroid belt at the time of OC parent body formation. We also propose that the D-rich (δD up to a minimum of 6000 ‰) component observed in UOCs of the lowest subtypes, which is very susceptible to even minor thermal or aqueous alteration, may correspond to amorphous silicates that were preserved from the molecular cloud or early protoplanetary disc.

## CRediT authorship contribution statement

**Helen Grant:** Writing – original draft, Visualization, Methodology, Investigation, Funding acquisition, Formal analysis, Conceptualization. **Romain Tartèse:** Writing – review & editing, Validation, Resources, Methodology, Funding acquisition, Formal analysis, Conceptualization. **Rhian Jones:** Writing – review & editing, Methodology, Funding acquisition, Conceptualization. **Laurette Piani:** Writing – review & editing, Resources, Methodology, Investigation, Formal analysis, Data curation. **Yves Marrocchi:** Writing – review & editing, Resources, Methodology, Investigation.

## Data availability

Raw and processed EPMA and SIMS data are available for download through FigShare at https://doi.org/10.48420/25828666.

## Declaration of competing interest

The authors declare that they have no known competing financial interests or personal relationships that could have appeared to influence the work reported in this paper.

## Acknowledgments

We thank Larry Nittler and two anonymous reviewers for their constructive feedback that improved this manuscript. We also acknowledge the UK Science and Technology Facilities Council for funding (ST/P005225/1 to R. T.; ST/V000675/1 to R. J., and studentship ST/T50628X/1 to H. G.). L.P. is thankful to the Agence Nationale de la Recherche (ANR) for its support through the grant ANR-19-CE31-0027-01 HYDRaTE (PI Laurette Piani). SIMS work was carried out with funding from the Europlanet 2024 RI which has received funding from the European Union's Horizon 2020 research and innovation programme under grant agreement No 871149. We thank Jonathan Fellowes (University of Manchester) and Michael Spilde (Institue of Meteoritics microprobe facility, University of New Mexico) for assistance with obtaining EPMA data, and the Natural History Museum (London), the American Museum of Natural History (NYC), and the Smithsonian Institution (Washington DC) for loans of the studied samples.

## Appendix A. Supplementary material

Supplementary material to this article can be found online at https://doi.org/10.1016/j.gca.2024.06.005 and downloadable tables can be found online at https://doi.org/10.48420/25828666.v1.

## References

Abreu, N.M., Brearley, A.J., 2010. Early solar system processes recorded in the matrices of two highly pristine CR3 carbonaceous chondrites, MET 00426 and QUE 99177. Geochim. Cosmochim. Acta 74, 1146–1171.
Alexander, C.M.O'D., Hutchison, R., Barber, D.J., 1989. Origin of chondrule rims and interchondrule matrices in unequilibrated ordinary chondrites. Earth *Planet. Sci. Lette.* 95 (3), 187–207.
Alexander, C.M.O'D., Fogel, M., Yabuta, H., Cody, G.D., 2007. The origin and evolution of chondrites recorded in the elemental and isotopic compositions of their macromolecular organic matter. Geochim. Cosmochim. Acta 71, 4380–4403.
Alexander, C.M.O., McKeegan, K.D., Altwegg, K., 2018. Water reservoirs in small planetary bodies: Meteorites, asteroids, and comets. Space Sci. Rev. 214, 36.
Alexander, C.M.O'D., Newsome, S.D., Fogel, M.L., Nittler, L.R., Busemann, H., Cody, G. D., 2010. Deuterium enrichments in chondritic macromolecular material—implications for the origin and evolution of organics, water and asteroids. Geochim. Cosmochim. Acta 74 (15), 4417–4437.
Alexander, C.M.O'D., Bowden, R., Fogel, M.L., Howard, K.T., Herd, C.D.K., Nittler, L.R., 2012. The provenances of asteroids, and their contributions to the volatile inventories of the terrestrial planets. Science 337 (6095), 721–723.
Bermingham, K.R., Füri, E., Lodders, K., Marty, B., 2020. The NC-CC isotope dichotomy: implications for the chemical and isotopic evolution of the early solar system. Space Sci. Rev. 216, 133.
Brearley, A.J., 1993. Matrix and fine-grained rims in the unequilibrated $CO_3$ chondrite, ALHA77307: Origins and evidence for diverse, primitive nebular dust components. Geochim. Cosmochim. Acta 57, 1521–1550.
Budde, G., Burkhardt, C., Brennecka, G.A., Fischer-Gödde, M., Kruijer, T.S., Kleine, T., 2016. Molybdenum isotopic evidence for the origin of chondrules and a distinct genetic heritage of carbonaceous and non-carbonaceous meteorites. Earth Planet. Sci. Lett. 454, 293–303.
Ceccarelli, C., Caselli, P., Bockelee-Morvan, D., Mousis, O., Pizzarello, S., Robert, F., Semenov, D., 2014. Deuterium fractionation: the Ariadne's thread from the precollapse phase to meteorites and comets today. In: Beuther, H., Klessen, R.S., Dullemond, C.P., Henning, T. (Eds.), Tuscon Protostars and Planets VI. University of Arizona Press, Arizona, pp. 859–883.
Carr, J.S., Najita, J.R., 2008. Organic molecules and water in the planet formation region of young circumstellar disks. Science 319, 1504–1506.
Che, S., Zega, T.J., 2023. Hydrothermal fluid activity on asteroid Itokawa. Nat. Astron 7, 1063–1069.
Christophe-Michel-Lévy, M., 1975. A few observations on the Tieschitz H3 chondrite. Meteorit. Planet. Sci. 10, 381.
Deligny, C., Füri, E., Deloule, E., 2021. Origin and timing of volatile delivery (N, H) to the angrite parent body: Constraints from in situ analyses of melt inclusions. Geochim. Cosmochim. Acta 313, 243–256.
Deloule, E., Robert, F., 1995. Interstellar water in meteorites? Geochim. Cosmochim. Acta 59, 4695–4706.
Dobrică, E., Brearley, A.J., 2014. Widespread hydrothermal alteration minerals in the fine-grained matrices of the Tieschitz unequilibrated ordinary chondrite. Meteorit. Planet. Sci. 49 (8), 1323–1349.
Dobrică, E., Brearley, A.J., 2020a. Amorphous silicates in the matrix of Semarkona: The first evidence for the localized preservation of pristine matrix materials in the most unequilibrated ordinary chondrites. Meteorit. Planet. Sci. 55, 649–668.
Dobrică, E., Brearley, A.J., 2020b. Iron-rich olivine in the unequilibrated ordinary chondrite, MET 00526: Earliest stages of formation. Meteorit. Planet. Sci. 55, 2652–2669.
Dodson-Robinson, S.E., Willacy, K., Bodenheimer, P., Turner, N.J., Beichman, C.A., 2009. Ice lines, planetesimal composition and solid surface density in the solar nebula. Icarus 200, 672–693.
Drouart, A., Dubrulle, B., Gautier, D., Robert, F., 1999. Structure and transport in the solar nebula from constraints on deuterium enrichment and giant planets formation. Icarus 140, 129–155.
Eschrig, J., Bonal, L., Beck, P., Prestgard, T.J., 2021. Spectral reflectance analysis of type 3 carbonaceous chondrites and search for their asteroidal parent bodies. Icarus 354, 114034.
Gattacceca, J., Suavet, C., Rochette, P., Weiss, B.P., Winklhofer, M., Uehara, M., Friedrich, J.M., 2014. Metal phases in ordinary chondrites: Magnetic hysteresis properties and implications for thermal history. Meteorit. Planet. Sci. 49, 652–676.
Geiss, J., Reeves, H., 1981. Deuterium in the solar system. Astron. Astrophys. 93, 189–199.
Grant, H., Tartèse, R., Jones, R., Piani, L., Marrocchi, Y., King, A., Rigaudier, T., 2023. Bulk mineralogy, water abundance, and hydrogen isotope composition of unequilibrated ordinary chondrites. Meteorit. Planet. Sci. 58 (9), 1365–1381.
Grossman, J.N., Brearley, A.J., 2005. The onset of metamorphism in ordinary and carbonaceous chondrites. Meteorit. Planet. Sci. 40 (1), 87–122.
Hallis, L.J., 2017. D/H ratios of the inner solar system. Philos. Transact. A Math. Phys. Eng. Sci. 375 (2094), 20150390.
Höfner, S., Olofsson, H., 2018. Mass loss of stars on the asymptotic giant branch. Astron. Astrophys. Rev. 26, 1.

Huss, G.R., Keil, K., Taylor, G.J., 1981. The matrices of unequilibrated ordinary chondrites: Implications for the origin and history of chondrites. Geochim. Cosmochim. Acta 45, 33–51.
Hutchison, R., Alexander, C.M.O'D., Barber, D.J., 1987. The Semarkona meteorite: First recorded occurrence of smectite in an ordinary chondrite, and its implications. Geochimica *Et Cosmochimica Acta* 51 (7), 1875–1882.
Ikeda, Y., Kimura, M., Mori, H., Takeda, H., 1981. Chemical compositions of matrices of unequilibrated ordinary chondrites. List of Memoirs of National Institute of Polar Research 20, 124–144.
Jacquet, E., Robert, F., 2013. Water transport in protoplanetary discs and the hydrogen isotopic composition of chondrites. Icarus 223, 722–732.
Jin, Z., Bose, M., 2019. New clues to ancient water on Itokawa. Sci. Adv. 5.
Jin, Z., Bose, M., Lichtenberg, T., Mulders, G.D., 2021. New evidence for wet accretion of inner Solar System planetesimals from meteorites Chelyabinsk and Benenitra. Planet. Sci. J. 2, 244.
Kleine, T., Budde, G., Burkhardt, C., Kruijer, T.S., Worsham, E.A., Morbidelli, A., Nimmo, F., 2020. The non-carbonaceous–carbonaceous meteorite dichotomy. Space Sci. Rev. 216, 55.
Krot, A.N., Doyle, P.M., Nagashima, K., Dobrică, E., Petaev, M.I., 2022. Mineralogy, petrology, and oxygen-isotope compositions of magnetite ± fayalite assemblages in CO3, CV3, and LL3 chondrites. Meteorit. Planet. Sci. 57, 392–428.
Kruijer, T.S., Burkhardt, C., Budde, G., Kleine, T., 2017. Age of Jupiter inferred from the distinct genetics and formation times of meteorites. Proc. Nat. Acad. Sci. 114, 6712–6716.
Le Guillou, C., Brearley, A., 2014. Relationships between organics, water and early stages of aqueous alteration in the pristine CR3.0 chondrite MET 00426. Geochim. Cosmochim. Acta 131, 344–367.
Le Guillou, C., Changela, H.G., Brearley, A.J., 2015. Widespread oxidized and hydrated amorphous silicates in CR chondrites matrices: Implications for alteration conditions and H2 degassing of asteroids. Earth Planet. Sci. Lett. 420, 162–173.
Leroux, H., Cuvillier, P., Zanda, B., Hewins, R.H., 2015. GEMS-like material in the matrix of the Paris meteorite and the early stages of alteration of CM chondrites. Geochim. Cosmochim. Acta 170, 247–265.
Marrocchi, Y., Bonal, L., Gattacceca, J., Piani, L., Beck, P., Greenwood, R., Eschrig, J., Basque, A., Nuccio, P.M., Martin, F.F., 2020. The Piancaldoli meteorite: A forgotten primitive LL3.10 ordinary chondrite. Meteorit. Planet. Sci. 55 (8), 1924–1935.
Marrocchi, Y., Avice, G., Barrat, J.-A., 2021. The Tarda meteorite: A window into the formation of D-type asteroids. Astrophys. J. Lett. 913, L9.
Marrocchi, Y., Rigaudier, T., Piralla, M., Piani, L., 2023. Hydrogen isotopic evidence for nebular pre-hydration and the limited role of parent-body processes in CM chondrites. Earth Planet. Sci. Lett. 611, 118151.
Matsunami, S., 1984. The chemical compositions and textures of matrices and chondrule rims of eight unequilibrated ordinary chondrites: A preliminary report. Memoirs Nat. Inst. Pol. Res., Special Issue 35, 126–148.
Matsuura, M., Dwek, E., Meixner, M., Otsuka, M., Babler, B., Barlow, M.J., Roman-Duval, J., Engelbracht, C., Sandstrom, K., Lakićević, M., van Loon, J.Th., Sonneborn, G., Clayton, G.C., Long, K.S., Lundqvist, P., Nozawa, T., Gordon, K.D., Hony, S., Panuzzo, P., Okumura, K., Misselt, K.A., Montiel, E., Sauvage, M., 2011. Herschel detects a massive dust reservoir in Supernova 1987A. Science 333, 1258.
McCubbin, F.M., Barnes, J.J., 2019. Origin and abundances of $H_2O$ in the terrestrial planets, Moon, and asteroids. Earth Planet. Sci. Lett. 526, 115771.
McCubbin, F.M., Lewis, J.A., Barnes, J.J., Elardo, S.M., Boyce, J.W., 2021. The abundances of F, Cl, and $H_2O$ in eucrites: Implications for the origin of volatile depletion in the asteroid 4 Vesta. Geochim. Cosmochim. Acta 314, 270–293.
McNaughton, N.J., Borthwick, J., Fallick, A.E., Pillinger, C.T., 1981. Deuterium/hydrogen ratios in unequilibrated ordinary chondrites. Nature 294 (5842), 639–641.
McNaughton, N.J., Borthwick, J., Fallick, A.E., Pillinger, C.T., 1982. Deuterium enrichments in primitive meteorites. J. Geophys. Res. Solid Earth 87 (S01), A297–A302.
Müller, D.R., Altwegg, K., Berthelier, J.J., Combi, M., De Keyser, J., Fuselier, S.A., Hänni, N., Pestoni, B., Rubin, M., Schroeder, I.R.H.G., Wampfler, S.F., 2022. High D/H ratios in water and alkanes in comet 67P/Churyumov-Gerasimenko measured with Rosetta/ROSINA DFMS. A & A 662, A69.
Nittler, L.R., Ciesla, F., 2016. Astrophysics with Extraterrestrial Materials. Ann. Rev. Astron. Astrophys. 54, 53–93.
Perotti, G., Christiaens, V., Henning, T., Tabone, B., Waters, L.B.F.M., Kamp, I., Olofsson, G., Grant, S.L., Gasman, D., Bouwman, J., Samland, M., Franceschi, R., van Dishoeck, E.F., Schwarz, K., Güdel, M., Lagage, P.-O., Ray, T.P., Vandenbussche, B., Abergel, A., Absil, O., Arabhavi, A.M., Argyriou, I., Barrado, D., Boccaletti, A., Caratti o Garatti, A., Geers, V., Glauser, A.M., Justannont, K., Lahuis, F., Mueller, M., Nehmé, C., Pantin, E., Scheithauer, S., Waelkens, C., Guadarrama, R., Jang, H., Kanwar, J., Morales-Calderón, M., Pawellek, N., Rodgers-Lee, D., Schreiber, J., Colina, L., Greve, T.R., Östlin, G., Wright, G., 2023. Water in the terrestrial planet-forming zone of the PDS 70 disk. Nature 620, 516–520.
Piani, L., Robert, F., Remusat, L., 2015. Micron-scale D/H heterogeneity in chondrite matrices: A signature of the pristine solar system water? Earth Planet. Sci. Lett. 415, 154–164.
Piani, L., Marrocchi, Y., 2018. Hydrogen isotopic composition of water in CV-type carbonaceous chondrites. Earth Planet. Sci. Lett. 504, 64–71.
Piani, L., Yurimoto, H., Remusat, L., 2018. A dual origin for water in carbonaceous asteroids revealed by CM chondrites. Nat. Astron 2, 317–323.
Piani, L., Marrocchi, Y., Rigaudier, T., Vacher, L.G., Thomassin, D., Marty, B., 2020. Earth's water may have been inherited from material similar to enstatite chondrite meteorites. Science 369, 1110–1113.
Piani, L., Marrocchi, Y., Vacher, L.G., Yurimoto, H., Bizzarro, M., 2021. Origin of hydrogen isotopic variations in chondritic water and organics. Earth Planet. Sci. Lett. 567, 117008.
Raymond, S., Izidoro, A., 2017. Origin of water in the inner Solar System: Planetesimals scattered inward during Jupiter and Saturn's rapid gas accretion. Icarus 297.
Remusat, L., Piani, L., Bernard, S., 2016. Thermal recalcitrance of the organic D-rich component of ordinary chondrites. Earth Planet. Sci. Lett. 435, 36–44.
Robert, F., Merlivat, L., Javoy, M., 1979. Deuterium concentration in the early Solar System: hydrogen and oxygen isotope study. Nature 282, 785–789.
Robert, F., Javoy, M., Halbout, J., Dimon, B., Merlivat, L., 1987. Hydrogen isotope abundances in the solar system. Part I: Unequilibrated chondrites. Geochim. Cosmochim. Acta 51 (7), 1787–1805.
Salyk, C., Pontoppidan, K.M., Blake, G.A., Lahuis, F., van Dishoeck, E.F., Evans II, N.J., 2008. $H_2O$ and OH gas in the terrestrial planet-forming zones of protoplanetary disks. Astrophys. J. 676, L49.
Sasselov, D.D., Lecar, M., 2000. On the snow line in dusty protoplanetary disks. Astrophys J 528, 995–998.
Scott, E.R.D., Krot, A.N., 2014. Chondrites and Their Components. In: Holland, H.D., Turekian, K.K. (Eds.), Treatise on Geochemistry, Second Edition. Elsevier, Oxford, pp. 65–137.
Scott, E.R.D., Krot, A.N., Sanders, I.S., 2018. Isotopic Dichotomy among Meteorites and Its Bearing on the Protoplanetary Disk. Astrophys J 854, 164.
Sears, D.W.G., Hasan, F.A., Batchelor, J.D., Lu, J., 1991. Chemical and physical studies of type 3 chondrites - XI: Metamorphism, pairing, and brecciation of ordinary chondrites. Lunar Planet. Sci. Conf. Proceedings 21, 493–512.
Sears, D.W.G., Morse, A.D., Hutchison, R., Guimon, R.K., Jie, L., Alexander, C.M.O., Benoit, P.H., Wright, I., Pillinger, C., Xie, T., Lipschutz, M.E., 1995. Metamorphism and aqueous alteration in low petrographic type ordinary chondrites. Meteoritics 30, 169–181.
Stephant, A., Remusat, L., Robert, F., 2017. Water in type I chondrules of Paris CM chondrite. Geochim. Cosmochim. Acta 199, 75–90.
Stephant, A., Zhao, X., Anand, M., Davidson, J., Carli, C., Cuppone, T., Pratesi, G., Franchi, I.A., 2023. Hydrogen in acapulcoites and lodranites: A unique source of water for planetesimals in the inner Solar System. Earth Planet. Sci. Lett. 615, 118202.
Vacher, L.G., Piani, L., Rigaudier, T., Thomassin, D., Florin, G., Piralla, M., Marrocchi, Y., 2020. Hydrogen in chondrites: Influence of parent body alteration and atmospheric contamination on primordial components. Geochim. Cosmochim. Acta 281, 53–66.
Vermeesch, P., 2018. IsoplotR: A free and open toolbox for geochronology. Geosci. Front. 9 (5), 1479–1493.
Warren, P.H., 2011a. Stable-isotopic anomalies and the accretionary assemblage of the Earth and Mars: A subordinate role for carbonaceous chondrites. Earth Planet. Sci. Lett. 311 (1), 93–100.
Warren, P.H., 2011b. Stable isotopes and the noncarbonaceous derivation of ureilites, in common with nearly all differentiated planetary materials. Geochim. Cosmochim. Acta 75, 6912–6926.
Weinberg, D., 2017. On the deuterium-to-hydrogen ratio of the interstellar medium. Astrophys J 851 (1), 25.
Weisberg, M.K., McCoy, T.J., Krot, A.N., 2006. Systematics and evaluation of meteorite classification. In: Lauretta, D.S., McSween, H.Y. (Eds.), Meteorites and the early solar system II. University of Arizona Press, Tuscon, Arizona, pp. 19–52.
Yang, L., Ciesla, F.J., Alexander, C.M.O'D., 2013. The D/H ratio of water in the solar nebula during its formation and evolution. Icarus 226 (1), 256–267.
Yang, J., Epstein, S., 1983. Interstellar organic matter in meteorites. Geochim. Cosmochim. Acta 47 (12), 2199–2216.
York, D., Evensen, N.M., Martínez, M.L., De Basabe, D.J., 2004. Unified equations for the slope, intercept, and standard errors of the best straight line. Am. J. Phys 72, 367–375.
Zanetta, P.-M., Le Guillou, C., Leroux, H., Zanda, B., Hewins, R.H., Bellino, G., 2022. Processes and temperatures of FGR formation in chondrites. Geochim. Cosmochim. Acta 319, 94–117.